

UC Berkeley

UC Berkeley Previously Published Works

Title

Prenol production in a microbial host via the “Repass” Pathways

Permalink

<https://escholarship.org/uc/item/263849m8>

Authors

Carruthers, David N

Donnell, Isaac

Sundstrom, Eric

et al.

Publication Date

2025-03-01

DOI

10.1016/j.ymben.2025.01.009

Copyright Information

This work is made available under the terms of a Creative Commons Attribution License, available at <https://creativecommons.org/licenses/by/4.0/>

Peer reviewed



Prenol production in a microbial host via the “Repass” Pathways

David N. Carruthers^{a,b}, Isaac Donnell^{b,c}, Eric Sundstrom^{a,d}, Jay D. Keasling^{a,b,e,f,g},
Taek Soon Lee^{a,b,*} 

^a Biological Systems & Engineering Division, Lawrence Berkeley National Laboratory, Berkeley, CA, USA

^b Joint BioEnergy Institute, 5885 Hollis Street, Emeryville, CA, USA

^c Department of Chemistry, University of California, Berkeley, CA, USA

^d Advanced Biofuels and Bioproducts Process Development Unit, Emeryville, CA, 94608, USA

^e Department of Chemical & Biomolecular Engineering, University of California, Berkeley, CA, USA

^f Department of Bioengineering, University of California, Berkeley, CA, USA

^g Center for Biosustainability, Danish Technical University, Lyngby, Denmark

ARTICLE INFO

Keywords:

Mevalonate pathway
Repass pathway
Isopentenyl phosphate kinase
Isopentenyl diphosphate isomerase
Prenol
Drupanin

ABSTRACT

Prenol and isoprenol are promising advanced biofuels and serve as biosynthetic precursors for pharmaceuticals, fragrances, and other industrially relevant compounds. Despite engineering improvements that circumvent intermediate cytotoxicity and lower energy barriers, achieving high titer ‘mevalonate (MVA)-derived’ prenol has remained elusive. Difficulty in selective prenol production stems from the necessary isomerization of isopentenyl diphosphate (IPP) to dimethylallyl diphosphate (DMAPP) as well as the intrinsic toxicity of these diphosphate precursors. Here, the expression of specific isopentenyl monophosphate kinases with model-guided enzyme substitution of diphosphate isomerases and phosphatases enabled selective cycling of monophosphates and diphosphates, dramatically improving prenol titers and selectivity in *Escherichia coli*. Pairing this approach with the canonical MVA pathway resulted in 300 mg/L prenol at a 30:1 ratio with isoprenol. Further pairing with the “IPP-Bypass” pathway resulted in 526 mg/L prenol at a 72:1 ratio with isoprenol, the highest and purest MVA-derived prenol titer to date. Additionally, modifying this “IPP-Repass” for DMAPP production and coexpressing the prenyltransferase acPT1 yielded 48.3 mg/L of the potential therapeutic precursor drupanin from p-coumarate. These novel repass pathways establish a unique strategy for tuning diphosphate precursors to drive isoprenoid biosynthesis and prenol reactions.

1. Introduction

Isoprenoids are mostly derived from either the methyl-4-erythritol phosphate (MEP) pathway or the mevalonate (MVA) pathway. Although evolutionarily distinct, both pathways generate the ubiquitous 5-carbon precursors isopentenyl diphosphate (IPP) and dimethylallyl diphosphate (DMAPP) with balancing via an isopentenyl diphosphate isomerase (IDI). Microbial isoprenoid bioproduction is predominantly accomplished via heterologous expression of the MVA pathway in bacterial hosts (Martin et al., 2003), a strategy that circumvents the complex intermediate feedback inhibition characteristic of bacterial MEP pathway refactoring (Li et al., 2020). Despite its own feedback inhibition mechanisms (Chen et al., 2017), decades of MVA pathway optimization have improved redox cofactor balancing (Tsuruta et al., 2009), reduced intermediate cytotoxicity (Ma et al., 2011), and led to the elucidation of

feedback-resistant enzymes (Primak et al., 2011).

Nonetheless, circumventing the cytotoxicity of the diphosphate intermediates has remained challenging (Li et al., 2018; Withers et al., 2007). Diphosphate intermediate toxicity is hypothesized to arise from condensation of the intermediates with ATP, forming the nucleotide analogue isoprenyl-ATP or AppI (George et al., 2018). Growth inhibition from diphosphate intermediate accumulation has proven sufficient to drive growth-coupled enzyme engineering of an isoprene synthase (Wang et al., 2017) as well as a mevalonate diphosphate decarboxylase (PMD) (Kang et al., 2017) for production of isoprene and isoprenol, respectively. In the latter study, the engineered PMD exhibited an improved promiscuous activity towards mevalonate monophosphate (MVAP), thereby directly generating isopentenyl monophosphate (IP) from MVAP and “bypassing” the production of toxic IPP (Kang et al., 2019). This “IPP-Bypass” pathway is capable of generating high titers of

* Corresponding author. Joint BioEnergy Institute, 5885 Hollis Street, Emeryville, CA, 94608, USA.

E-mail address: tslee@lbl.gov (T.S. Lee).

<https://doi.org/10.1016/j.ymben.2025.01.009>

Received 17 September 2024; Received in revised form 17 January 2025; Accepted 24 January 2025

Available online 25 January 2025

1096-7176/© 2025 The Authors. Published by Elsevier Inc. on behalf of International Metabolic Engineering Society. This is an open access article under the CC BY license (<http://creativecommons.org/licenses/by/4.0/>).

isoprenol, an appealing gasoline blend additive and a precursor to the sustainable aviation fuel 1,4-dimethylcyclooctane (DMCO) (Baral et al., 2021; Rosenkoetter et al., 2019). However, the IPP-bypass strictly limits the pathway to isoprenol while prenol remains an appealing gasoline blend additive and precursor to other chemicals (Carruthers et al., 2023; Monroe et al., 2019).

Recently, isoprenoid alcohol utilization pathways were developed as alternatives to the canonical MVA pathway (Chatzivasileiou et al., 2019; Clomburg et al., 2019). One pathway was engineered through a *de novo* approach, ultimately arriving upon a five enzyme cascade (LiuC, AibA, AibB, and cbjALD from *Myxococcus xanthus* and YahK from *E. coli*) to generate high prenol titers from 3-hydroxy-3-methylglutaryl coenzyme-A (HMG-CoA) (Clomburg et al., 2019). Then, endogenous prenol is then sequentially converted into DMAP and DMAPP by co-expression of an *E. coli* hydroxyethylthiazole kinase (thiM) and an archaeal isopentenyl monophosphate kinase (IPK), respectively (Clomburg et al., 2019). Another pathway involved a two-step process where co-expression of a choline kinase from *Saccharomyces cerevisiae* and an IPK from *Arabidopsis thaliana* with addition of exogenous isoprenol and prenol yield their respective mono and then diphosphates

(Chatzivasileiou et al., 2019).

The isoprenoid alcohol utilization pathways reframe C5 alcohols as intermediates rather than products. Of crucial relevance are their inclusion of highly active IPKs, which are integral to archaeal MVA pathways and tend to favor IP as a substrate (Dellas et al., 2013). Two archaeal IPKs from *Methanothermobacter thermoautotrophicus* and *Thermoplasma acidophilum* have been kinetically characterized *in vitro* (Chen and Poulter, 2010) with IPK_{Ta} further mutagenized for geranyl monophosphate kinase activity (Mabanglo et al., 2012), prenol kinase activity (Liu et al., 2016), and expressed to provide stringent growth-coupling in IPP-bypass pathway engineering (Kang et al., 2017).

Here, we engineered two extensively optimized MVA pathways (the “Original” MVA pathway and the “IPP-bypass” pathway) with a library of phosphatases, kinases, and isomerases to recycle isopentenyl/prenol monophosphates with their respective diphosphates in the purported “Original-Repass” and “IPP-Repass” pathways (Fig. 1).

While the phosphatase and isomerase act on both DMAPP and IPP and the kinase acts on both DMAP and IP, we leveraged the reported *in vitro* selectivity of IPK_{Mt} and IPK_{Ta} towards IP over DMAP (64% and 96.4%, respectively) (Chen and Poulter, 2010) to significantly increase

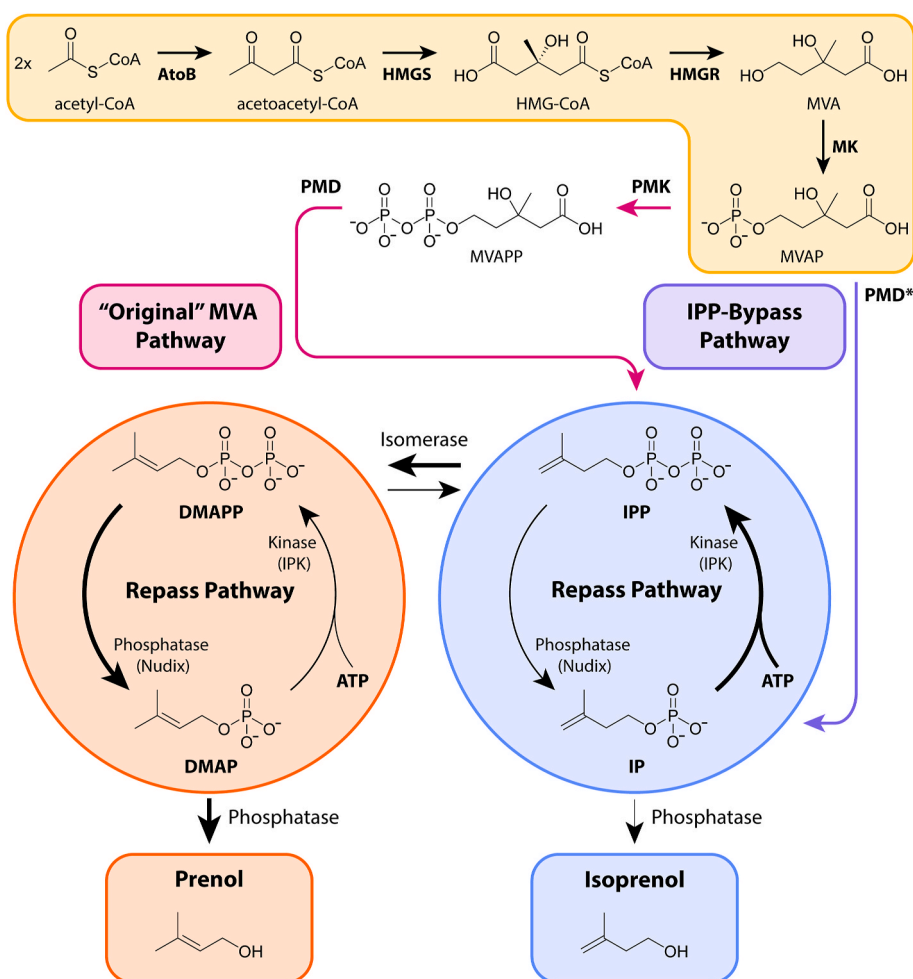


Fig. 1. An overview of the repass pathways. The canonical MVA pathway (yellow box) condenses two acetyl-CoA precursors via an acetyltransferase to generate acetoacetyl-CoA. Acetoacetyl-CoA is converted into hydroxymethylglutaryl-CoA (HMG-CoA) by HMG-CoA synthase, then reduced to mevalonic acid (MVA) by HMG-CoA reductase and then phosphorylated to mevalonate monophosphate by mevalonate kinase (MK). The pathways diverge with the “Original MVA” pathway (magenta line) proceeding to mevalonate diphosphate via a mevalonate monophosphate kinase (PMK) then to IPP via mevalonate decarboxylase (PMD). Alternatively, the “IPP-Bypass” pathway (violet line) utilizes a promiscuous decarboxylase, (PMD*) to directly convert MVAP into IP. These pathways are characterized by their final metabolite, IPP for the Original MVA pathway and IP for the IPP-Bypass pathway. When paired with a phosphatase, isomerase, and kinase, these MVA pathways become the Original-Repass and IPP-Repass pathways. The recycling of metabolites by the kinase, isomerase, and phosphatase may be subdivided into DMAP/DMAPP recycling (orange circle) and IPP/IP cycling (blue circle) with flux towards a terminal alcohol derived from the interplay of enzyme kinetics. Repass pathway line width denotes proposed flux.

flux towards DMAPP and ultimately prenol. Then, using simple enzyme kinetics, we evaluated pathway sensitivity to isomerase and phosphatase kinetics. By exploring enzymes across different evolutionary domains, we discovered a combination capable of generating 526 mg/L prenol in a 72:1 ratio of prenol to isoprenol, which is the highest titer and purity of canonically MVA-derived prenol to date. Finally, a Repass pathway was paired with a selected prenyltransferase, acPT1, to demonstrate its capacity to drive prenylation reactions. Such reactions are crucial for generating certain small natural product derivatives from indole alkaloids (Li, 2010), isoprenoids, and other aromatics, yet are often limited by DMAPP supply (Munakata et al., 2019). Our successful production of drupanin suggests that the repass pathways may be able to drive a variety of other prenylation schemes. Overall, the repass pathways represent a significant new development in MVA pathway engineering.

2. Materials and methods

2.1. Construction of plasmids and strains

Plasmids were assembled by amplifying genes and vectors from the JBEI Registry, apart from the isomerases from *T. acidophilum* and *Methanosarcina mazei*, which were codon optimized for *Escherichia coli* (Twist Biosciences, South San Francisco). Specifically, genes of interest were amplified via PCR using Q5 DNA polymerase (New England Biolabs (NEB), Ipswich, MA) and oligos (Integrated DNA Technologies, Redwood City, CA) with respective 15–30 bp 5' overhangs for downstream assembly. Amplicons were purified (QIAquick PCR Purification Kit, Qiagen Inc., Germantown, MD), digested with *dpnI* (Thermo Fisher Scientific, Waltham, MA), assembled (NEBuilder HiFi DNA Assembly Cloning Kit, NEB), and cloned into chemically competent XL-1 Blue *E. coli* cells prepared by the UC Berkeley QB3 Core facility (Berkeley, CA). Successful transformants were screened with routine PCR (OneTaq, NEB), miniprep (QIAPrep Spin Miniprep Kit, Qiagen), and analyzed for sequence fidelity using either Sanger sequencing (Azenta Life Sciences, Burlington, MA) or whole plasmid sequencing (Primordium Labs, Monrovia, CA) depending on construct size. Following successful sequence validation, plasmids were transformed (2500 V, 5 ms) via 2 mm cuvettes (BioRad Inc, Hercules, CA) into electrochemically competent *E. coli* production strains.

E. coli DH1 was selected owing to its historic use for isoprenoid production. A secondary strain was also constructed harboring a hydroxyethylthiazole kinase (*thiM*) deletion, which is the gene responsible for conversion of prenol into DMAP (Clomburg et al., 2019). The deletion strain was constructed by cloning a pSIM5 into *E. coli* DH1. Briefly, pSIM5 harbors lambda-red recombining genes under a lambda phage promoter controlled by the cI857 temperature-sensitive repressor. Overnight culture was diluted 100-fold into fresh LB with 25 mg/L chloramphenicol and grown to an OD₆₀₀ of 0.4 at 30 °C. Lambda-red genes were induced through incubation at 42 °C for 15 min followed by immediate cooling in an ice slurry. The *ΔthiM* locus was amplified from the specified Keio Collection strain (JW 2091 (Baba et al., 2006)). Linearized single-stranded DNA was then transformed into electrocompetent DH1 expressing lambda-red genes and plated on 50 mg/L kanamycin. Following curing of pSIM5 at 42 °C, the embedded kanamycin resistance marker in *ΔthiM* was removed via FLP recombination by transformation and subsequent expression of pCP20. Finally, the strain was cured by culturing at 42 °C to yield DH1 *ΔthiM*.

Plasmids constructed and used in this work are described in Table 1 and are available in the public domain of the JBEI Registry (<http://public-registry.jbei.org>).

2.2. Repass production culture conditions

All production screens were performed using freshly transformed strains. For each assay, a single colony was inoculated into 5 mL of Luria-

Table 1
Strains and plasmids used in this study.

Plasmid or Strain	JBEI Registry Part ID	Genotype	Ref
<i>Strain</i>			
DH1	–	F [−] λ [−] endA1 recA1 relA1 gyrA96 thi-1 glnV44 hsdR17 (r _K m _K)	Wild type
JW2091	JBEI-006176	F [−] Δ(araD-araB)567, ΔlacZ4787(rrmB-3), λ [−] , ΔthiM729:kan, rph-1, Δ(rhaD-rhaB)568, hsdR514	Baba et al. (2006)
DH1 <i>ΔthiM</i>	JBEI-261224	F [−] λ [−] endA1 recA1 relA1 gyrA96 thi-1 glnV44 hsdR17 (r _K m _K) <i>ΔthiM</i>	This work
BL21	–	F-ompT hsdSB (r _B , m _B) gal dcm (DE3)	Wild type
BL21 Star (DE3)	–	F-ompT hsdSB (r _B , m _B) gal dcm rne1.31 (DE3)	Invitrogen™
<i>Plasmid</i>			
pCP20	JBEI-7585	repA101 ^{ts} , FLP recombinase expression	Cherepanov and Wackernagel (1995)
pSIM5	JBEI-14339	repA101 ^{ts} , λ-Red recombining	Datta et al. (2006)
Upper IPP-Bypass	JBEI-17081	pBbA5c-atoB-HMGs _{Sa} -HMG _{Rsa}	Ma et al. (2011)
Upper OriMVA IPP-Bypass	JBEI-6829	pBbA5c-atoB-HMGs _{Sa} -HMG _{Rsa} -MK _{Sc} -PMK _{Sc}	George et al. (2014)
	JBEI-17844	pTrc99a-PMD ^{Sc} -MK _{Mm}	Kang et al. (2017)
pDNC7 (OriRe-Control)	JBEI-231871	pTrc99A-nudB-IDI1 _{Sc} -PMD _{Sc}	Carruthers et al. (2023)
OriRe-LacUV5-IPK _{Mt}	JBEI-260975	pTrc99A-nudB-IDI1 _{Sc} -PMD _{Sc} -LacUV5-IPK _{Mt}	This work
OriRe-IPK _{Mt}	JBEI-260976	pTrc99A-nudB-IDI1 _{Sc} -PMD _{Sc} -IPK _{Mt}	This work
OriRe-LacUV5-IPK _{Ta}	JBEI-260977	pTrc99A-nudB-IDI1 _{Sc} -PMD _{Sc} -LacUV5-IPK _{Ta}	This work
OriRe-IPK _{Ta} (aka OriRe)	JBEI-260978	pTrc99A-nudB-IDI1 _{Sc} -PMD _{Sc} -IPK _{Ta}	This work
OriRe-PMD _{Sc}	JBEI-260979	pTrc99A-nudB-IDI1 _{Sc} -PMD _{Sc}	This work
OriRe-PMD _{Sc} -LacUV5-IPK _{Mt}	JBEI-260980	pTrc99A-nudB-IDI1 _{Sc} -PMD _{Sc} -LacUV5-IPK _{Mt}	This work
OriRe-PMD _{Sc} -LacUV5-IPK _{Ta}	JBEI-260981	pTrc99A-nudB-IDI1 _{Sc} -PMD _{Sc} -LacUV5-IPK _{Ta}	This work
OriRe-nudA	JBEI-260982	pTrc99A-nudA-IDI1 _{Sc} -PMD _{Sc} -IPK _{Ta}	This work
OriRe-nudC	JBEI-260983	pTrc99A-nudC-IDI1 _{Sc} -PMD _{Sc} -IPK _{Ta}	This work
OriRe-nudD	JBEI-260984	pTrc99A-nudD-IDI1 _{Sc} -PMD _{Sc} -IPK _{Ta}	This work
OriRe-nudE	JBEI-261220	pTrc99A-nudE-IDI1 _{Sc} -PMD _{Sc} -IPK _{Ta}	This work
OriRe-nudF	JBEI-261221	pTrc99A-nudF-IDI1 _{Sc} -PMD _{Sc} -IPK _{Ta}	This work
OriRe-nudG	JBEI-261223	pTrc99A-nudG-IDI1 _{Sc} -PMD _{Sc} -IPK _{Ta}	This work
OriRe-nudH	JBEI-261224	pTrc99A-nudH-IDI1 _{Sc} -PMD _{Sc} -IPK _{Ta}	This work
OriRe-nudI	JBEI-260989	pTrc99A-nudI-IDI1 _{Sc} -PMD _{Sc} -IPK _{Ta}	This work
OriRe-nudJ	JBEI-260990	pTrc99A-nudJ-IDI1 _{Sc} -PMD _{Sc} -IPK _{Ta}	This work
OriRe-nudK	JBEI-260991	pTrc99A-nudK-IDI1 _{Sc} -PMD _{Sc} -IPK _{Ta}	This work
OriRe-nudL	JBEI-260992	pTrc99A-nudL-IDI1 _{Sc} -PMD _{Sc} -IPK _{Ta}	This work

(continued on next page)

Table 1 (continued)

Plasmid or Strain	JBEI Registry Part ID	Genotype	Ref
OriRe-nudM	JBEI-260993	pTrc99A-nudM-IDI1 _{Sc} -PMD _{Sc} -IPK _{Ta}	This work
OriRe-aphA	JBEI-260994	pTrc99A-aphA-IDI1 _{Sc} -PMD _{Sc} -IPK _{Ta}	This work
OriRe-IDI2 _{Bs}	JBEI-260995	pTrc99A-nudB-IDI2 _{Bs} -PMD _{Sc} -IPK _{Ta}	This work
OriRe-IDI2 _{Bl}	JBEI-260996	pTrc99A-nudB-IDI2 _{Bl} -PMD _{Sc} -IPK _{Ta}	This work
OriRe-IDI1 _{Ec}	JBEI-260997	pTrc99A-nudB-IDI1 _{Ec} -PMD _{Sc} -IPK _{Ta}	This work
OriRe-IDI2 _{Sa}	JBEI-260998	pTrc99A-nudB-IDI2 _{Sa} -PMD _{Sc} -IPK _{Ta}	This work
OriRe-IDI2 _{At}	JBEI-260999	pTrc99A-nudB-IDI2 _{At} -PMD _{Sc} -IPK _{Ta}	This work
OriRe-IDI2 _{Ta}	JBEI-261000	pTrc99A-nudB-IDI2 _{Ta} -PMD _{Sc} -IPK _{Ta}	This work
OriRe-IDI2 _{Mm}	JBEI-261001	pTrc99A-nudB-IDI2 _{Mm} -PMD _{Sc} -IPK _{Ta}	This work
OriRe-nudJ-IDI2 _{Bs}	JBEI-261002	pTrc99A-nudJ-IDI2 _{Bs} -PMD _{Sc} -IPK _{Ta}	This work
OriRe-nudJ-IDI2 _{Bl}	JBEI-261003	pTrc99A-nudJ-IDI2 _{Bl} -PMD _{Sc} -IPK _{Ta}	This work
IPPre (IPP-Repas)	JBEI-261004	pTrc99A-nudB-IDI1 _{Sc} -PMD* _{Sc} -MK _{Mm} -IPK _{Ta}	This work
IPPre-LacUV5-IPK _{Mt}	JBEI-261005	pTrc99A-nudB-IDI1 _{Sc} -PMD* _{Sc} -MK _{Mm} -LacUV5-IPK _{Mt}	This work
IPPre-IPK _{Mt}	JBEI-261006	pTrc99A-nudB-IDI1 _{Sc} -PMD* _{Sc} -MK _{Mm} -IPK _{Mt}	This work
IPPre-LacUV5-IPK _{Ta}	JBEI-261007	pTrc99A-nudB-IDI1 _{Sc} -PMD* _{Sc} -MK _{Mm} -LacUV5-IPK _{Ta}	This work
IPPre-nudA	JBEI-261008	pTrc99A-nudA-IDI1 _{Sc} -PMD* _{Sc} -MK _{Mm} -IPK _{Ta}	This work
IPPre-nudC	JBEI-261009	pTrc99A-nudC-IDI1 _{Sc} -PMD* _{Sc} -MK _{Mm} -IPK _{Ta}	This work
IPPre-nudD	JBEI-261010	pTrc99A-nudD-IDI1 _{Sc} -PMD* _{Sc} -MK _{Mm} -IPK _{Ta}	This work
IPPre-nudE	JBEI-261011	pTrc99A-nudE-IDI1 _{Sc} -PMD* _{Sc} -MK _{Mm} -IPK _{Ta}	This work
IPPre-nudF	JBEI-261012	pTrc99A-nudF-IDI1 _{Sc} -PMD* _{Sc} -MK _{Mm} -IPK _{Ta}	This work
IPPre-nudG	JBEI-261013	pTrc99A-nudG-IDI1 _{Sc} -PMD* _{Sc} -MK _{Mm} -IPK _{Ta}	This work
IPPre-nudH	JBEI-261014	pTrc99A-nudH-IDI1 _{Sc} -PMD* _{Sc} -MK _{Mm} -IPK _{Ta}	This work
IPPre-nudI	JBEI-261015	pTrc99A-nudI-IDI1 _{Sc} -PMD* _{Sc} -MK _{Mm} -IPK _{Ta}	This work
IPPre-nudJ	JBEI-261016	pTrc99A-nudJ-IDI1 _{Sc} -PMD* _{Sc} -MK _{Mm} -IPK _{Ta}	This work
IPPre-nudK	JBEI-261017	pTrc99A-nudK-IDI1 _{Sc} -PMD* _{Sc} -MK _{Mm} -IPK _{Ta}	This work
IPPre-nudL	JBEI-261018	pTrc99A-nudL-IDI1 _{Sc} -PMD* _{Sc} -MK _{Mm} -IPK _{Ta}	This work
IPPre-nudM	JBEI-261019	pTrc99A-nudM-IDI1 _{Sc} -PMD* _{Sc} -MK _{Mm} -IPK _{Ta}	This work
IPPre-aphA	JBEI-261020	pTrc99A-aphA-IDI1 _{Sc} -PMD* _{Sc} -MK _{Mm} -IPK _{Ta}	This work
IPPre-IDI2 _{Bs}	JBEI-261021	pTrc99A-nudB-IDI2 _{Bs} -PMD* _{Sc} -MK _{Mm} -IPK _{Ta}	This work
IPPre-IDI2 _{Bl}	JBEI-261022	pTrc99A-nudB-IDI2 _{Bl} -PMD* _{Sc} -MK _{Mm} -IPK _{Ta}	This work
IPPre-IDI1 _{Ec}	JBEI-261023	pTrc99A-nudB-IDI1 _{Ec} -PMD* _{Sc} -MK _{Mm} -IPK _{Ta}	This work
IPPre-IDI2 _{Sa}	JBEI-261024	pTrc99A-nudB-IDI2 _{Sa} -PMD* _{Sc} -MK _{Mm} -IPK _{Ta}	This work
IPPre-IDI2 _{At}	JBEI-261025	pTrc99A-nudB-IDI2 _{At} -PMD* _{Sc} -MK _{Mm} -IPK _{Ta}	This work
IPPre-IDI2 _{Ta}	JBEI-261026	pTrc99A-nudB-IDI2 _{Ta} -PMD* _{Sc} -MK _{Mm} -IPK _{Ta}	This work
IPPre-IDI2 _{Mm}	JBEI-261027	pTrc99A-nudB-IDI2 _{Mm} -PMD* _{Sc} -MK _{Mm} -IPK _{Ta}	This work
IPPre-Control	JBEI-261028	pTrc99A-nudJ-IDI1 _{Sc} -PMD _{Sc} -MK _{Mm} -PMK _{Sc}	This work

Table 1 (continued)

Plasmid or Strain	JBEI Registry Part ID	Genotype	Ref
ATF1-Control	JBEI-261029	pTrc99A-nudB-IDI2 _{Bs} -PMD _{Sc} -PMK _{Sc} -LacUV5-ATF1	This work
ATF1-OriRe	JBEI-261030	pTrc99A-nudB-IDI2 _{Bs} -PMD _{Sc} -IPK-LacUV5-ATF1	This work
ATF1-IPPre	JBEI-261031	pTrc99A-nudJ-IDI1 _{Sc} -PMD* _{Sc} -MK _{Mm} -IPK-LacUV5-ATF1	This work
acPT1co1	JBEI-261032	pBbs8k-acPT1co1	This work
acPT1co2 (acPT1)	JBEI-261033	pBbs8k-acPT1co2	This work
acPT1-Control	JBEI-261034	pTrc99A-IDI1 _{Sc} -PMD* _{Sc} -MK _{Mm}	This work
acPT1-IPPre	JBEI-261035	pTrc99A-IDI1 _{Sc} -PMD* _{Sc} -MK _{Mm} -IPK _{Ta}	This work
RFP-Control	JBEI-2499	pBbs8k-RFP	Lee et al. (2011)

Bertani (LB) Miller medium (10 g/L tryptone, 5 g/L yeast extract and 10 g/L sodium chloride) with appropriate antibiotics (100 mg/L carbenicillin, 25 mg/L chloramphenicol, or 50 mg/L kanamycin). Following overnight growth at 37 °C at 200 RPM on a rotary shaker, 200 µL of seed culture was inoculated into the production medium in triplicate. The production medium included M9 salts (6.78 g/L Na₂HPO₄, 3 g/L KH₂PO₄, 1 g/L NH₄Cl, and 0.5 g/L NaCl), 1 mg/L thiamine, 2 mM MgSO₄, 10 µM FeSO₄, 0.1 mM CaCl₂, micronutrients (3*10⁻⁸ M (NH₄)₆Mo₇O₂₄, 4*10⁻⁶ M boric acid, 3*10⁻⁷ M CoCl₂, 1.5*10⁻⁷ M CuSO₄, 8*10⁻⁷ M MnCl₂, and 1*10⁻⁷ M ZnSO₄), as well as 75 mM 3-morpholinopropane-1-sulfonic acid (MOPS), 20 g/L glucose, appropriate antibiotics, and, if stated, 5 g/L yeast extract.

Cultures for isopentenol production were inoculated and grown at 37 °C at 200 RPM on a rotary shaker, then induced at an OD₆₀₀ (optical density at 600 nm with 1 cm path length) between 0.4 and 0.6 with 0.5 mM isopropyl β-D-1-thiogalactopyranoside (IPTG). Strains were then grown at 30 °C and 200 rpm. Isopentenol production did not require an overlay. An oleyl alcohol overlay was used exclusively for isoprenyl and prenyl acetate production cultures to avoid excessive product evaporation. Unless otherwise stated, production in 5 mL culture tubes was measured after 72 h with OD₆₀₀ measured at induction and 72 h. Strains for prenylated compound production were instead induced at an OD₆₀₀ between 0.6 and 0.8 by addition of 500 mM IPTG and 2 g/L L-arabinose for MVA pathway and acPT1 expression, respectively. A 0.5 M stock solution of p-coumarate was prepared by continuously stirring p-coumaric acid (Sigma-Aldrich) into deionized water, followed by titration with NaOH until the pH reached 8.6. The dissolved solution was then sterilized through a 0.22 µm cellulose acetate membrane filter. At induction, 1 g/L p-coumarate was also added to enable drupanin biosynthesis. Prenylated production cultures were scaled to 200 mL in 1 L flasks to amass enough product for NMR spectroscopy.

2.3. Quantification of isoprenoids by gas chromatography

Upon sampling, culture cells, aqueous medium, and, where applicable, overlay were separated by centrifugation at 13,000×g for 5 min. Following centrifugation, 400 µL of aqueous phase was mixed with 400 µL of ethyl acetate with 30 mg/L 1-butanol internal standard and vortexed for 10 min at 3000 RPM (Scientific industries INC, USA). The aqueous phase and ethyl acetate mixture was then centrifuged again at 13,000×g for 5 min and 200 µL of the ethyl acetate extraction was then aliquoted into labeled GC vials with glass inserts for chromatography. Prenyl and isoprenyl acetate production required the addition of a nonpolar organic overlay, oleyl alcohol, to reduce evaporation and sequester product. There, 10 µL of overlay was carefully removed and added to 990 µL of ethyl acetate with internal standard for a 1:100 final concentration.

Isoprenoids were detected by gas chromatography - flame ionization detection (GC-FID) using an Agilent 8890 with a DB-Wax column (Agilent 123–7012; 15 m length, 320 μm diameter, and 0.25 μm film thickness). The acquisition method included an inlet temperature of 250 $^{\circ}\text{C}$, detector temperature of 300 $^{\circ}\text{C}$, and 2.2 mL/min helium mobile phase flow. The oven program consisted of an initial 1-min hold at 40 $^{\circ}\text{C}$, a ramp of 15 $^{\circ}\text{C}/\text{min}$ to 100 $^{\circ}\text{C}$, a 30 $^{\circ}\text{C}/\text{min}$ ramp rate to 230 $^{\circ}\text{C}$, and a final 1-min hold at 230 $^{\circ}\text{C}$. Normalized analyte peak areas were compared against analytical grade standards run using the same acquisition method.

2.4. Expression of acPT1

The full coding sequence of acPT1 from *Artemisia capillaris* as well as two truncated sequences acPT1co1 ($\Delta 150$ bp) and acPT1co2 ($\Delta 243$) were codon optimized for *S. cerevisiae*. Sequences were truncated from the N-terminus owing to remove the native transit peptide sequence. Each sequence was fused with RFP and cloned into *E. coli* strains DH1, BL21, and BL21(star) to ascertain protein localization. Images were acquired using a Zeiss LSM 710 confocal microscope (Thermo Fisher Scientific) (Fig. S4). Microscopy indicated no fluorescence in strains harboring acPT1 or acPT1co1. Conversely, acPT1co2 demonstrated minor and moderate fluorescence in *E. coli* DH1 and BL21, respectively. Localization appeared comparable though attenuated compared to RFP only controls, which provided compelling evidence for successful protein expression and further supported by soluble fraction partitioning of RFP-tagged acPT1co2 during protein extraction.

2.5. Characterization of acPT1 derived products

Phenolic compounds were extracted according to previously described methods (Munakata et al., 2019). Briefly, 5 mL cultures were centrifuged at $3000\times g$ for 10 min. The supernatant was aliquoted into a separate tube and the cell pellet was resuspended in 5 mL DI H_2O . Then 1 mL of each fraction was mixed with 200 μL of 3 N HCl and 1 mL of ethyl acetate and vortexed for 2 min. Aqueous and organic fractions were separated by centrifugation at $15,000\times g$ for 5 min. After centrifugation, 500 μL of organic phase was separated and dried (Centrивap Concentrator, LABCONCO). Dried organic phase was resuspended in 500 μL of MeOH, centrifuged at $15,000\times g$ for 5 min, and 250 μL was subjected to high performance liquid chromatography (HPLC; Agilent Technologies). The mobile phase consisted of 0.1% (v/v) formic acid in water (solvent A) and 0.1% (v/v) formic acid in methanol (solvent B). Initially, 80% solvent A and 20% solvent B was run for 2.5 min, then graduated to 90% solvent B over 15 min and 100% solvent B over 5 min and then steady for an additional 7.5 min before returning to initial conditions. The flow rate was maintained at 1 mL/min with an oven temperature of 40 $^{\circ}\text{C}$. A diode array detector was used to monitor phenolic compounds at 315 nm.

Phenolic extracts were further analyzed using high-performance LC–MS (HPLC–MS) using an Agilent 1260 infinity II system with mass selective detector XT (MSD XT). The HPLC autosampler and column compartment were maintained at 10 $^{\circ}\text{C}$ and 25 $^{\circ}\text{C}$, respectively. A Macherey Nagel Sphinx RP column (5 μm , 4.6 mm \times 150 mm) was used for analysis. The mobile phase consisted of 0.1% (v/v) formic acid in water (solvent A) and 0.1% (v/v) formic acid in acetonitrile (solvent B). The column was eluted with a gradient of 2% B to 100% B over 15 min, held at 100% B for 1 min for separation and analysis, then reduced to 2% B for 9 min to equilibrate the column.

Drupanin was extracted from five 1 L flasks with 200 mL medium cultured over 72 h. Using the aforementioned extraction protocol, the extract was separated using semi-preparative HPLC with a RediSep C18 Column (5 μm , 250 mm \times 10 mm), suspected fractions containing drupanin were confirmed via HPLC, then combined and dried. The collected 3.5 mg of purified extract was resuspended in 250 μL of methanol- d_4 , placed in a solvent matched 5 mm Shigemi NMR tube and

analyzed using a Bruker NEO-500. The NMR spectra (^1H , ^{13}C , NOESY, HSQC; Figs. S6–S9) matched that of the drupanin spectra in the literature, confirming its identity (Rodrigues et al., 2021).

2.6. Kinetic modeling

A kinetic model was built with the SciPy library (Virtanen et al., 2020) in Python 3.10.6 using a Jupyter Notebook (Supplementary Information). The model consists of 8 ordinary differential equations, one equation for each of the 8 reactions. In order to use Michaelis-Menten kinetics, we assumed that each reaction has a constant rate of product formation, that the substrate concentration is typically higher than enzyme concentration, and that the reactions are irreversible. Given that we are under highly aerobic conditions, we also approximated the kinase reactions as single substrate reactions by assuming that ATP is not limiting. Several deep learning models were explored for enzyme kinetics, however these failed to reflect observed performance (e.g., IPK_{Ta} vs. IPK_{Mt} selectivity for IP vs. DMAP).

3. Results and discussion

3.1. Repass pathway overview

The Original MVA pathway (OriMVA) and IPP-Bypass pathways were investigated for pathway engineering. As illustrated in Fig. 1, both pathways begin with a Claisen condensation of two acetyl-CoA precursors by an acetyl-CoA acetyltransferase (AtoB, *E. coli*) to generate acetoacetyl-CoA, which is sequentially converted to hydroxymethylglutaryl-CoA (HMG-CoA) by a HMG-CoA synthase (HMGS, *S. aureus*) and to mevalonic acid (MVA) by an HMG-CoA reductase (HMGR, *S. aureus*). A codon optimized mevalonate kinase (MK, *S. cerevisiae*) and mevalonate monophosphate kinase (PMK, *S. cerevisiae*) sequentially phosphorylate MVA to MVAPP. Taken together, these enzymes collectively comprise the upper OriMVA pathway (Fig. 2A). Subsequent expression of a decarboxylase (PMD, *S. cerevisiae*) ultimately converts MVAPP to IPP, which may be further converted to isoprenol by phosphatases such as NudB (*E. coli*) or to prenil through coexpression of an IDI1 (*S. cerevisiae*) via DMAPP. While the upper OriMVA pathway is expressed by IPTG induction on a low copy plasmid (Upper OriMVA, JBEI-6829; (George et al., 2014)), the lower OriMVA pathway is expressed on a high copy plasmid (pDNC7, JBEI-231871; (Carruthers et al., 2023)).

Conversely, the IPP-Bypass pathway has a mutated PMD* (*S. cerevisiae*) with characteristic promiscuity towards MVAP to directly generate IP. The pathway circumvents PMK expression and, as a result, bypasses the formation of toxic IPP while saving an ATP in the process. Structurally, the upper IPP-Bypass pathway enzymes AtoB, HMGS, and HMGR (Fig. 2A) are expressed by IPTG induction on a low copy plasmid (JBEI-17081), while codon optimized MK (*M. mazei*) and PMD* are coexpressed on a high copy plasmid (JBEI-17844 (Kang et al., 2016)).

Two IPK enzymes originating from *M. thermotrophicus* and *T. acidophilum* were selected owing to their promising *in vitro* kinetic characterization (Chen and Poulter, 2010). Pairing the OriMVA pathway with an IPK yields the Ori-Repass pathway. The analogous IPP-Repass pathway requires further expression of nudB and IDI1. Although contrary in principle to the IPP-Bypass pathway, we considered whether cycling of monophosphates and diphosphates in an IPP-Repass pathway could also enhance prenil titer as, with the addition of an IPK, it remains enzymatically shorter though now energetically equal to the original pathway.

Summarily, the lower pathway consists of a strong IPTG inducible promoter, phosphatase, isomerase, and decarboxylase then either IPK (Ori-Repass; OriRe) or MK then IPK (IPP-Repass; IPPRe). We used capitalized “Repass” to describe a specific pathway (e.g., Ori-Repass, IPP-Repass) and “repass” to describe the overall approach. These configurations of the Ori-Repass and IPP-Repass facilitated rapid assembly

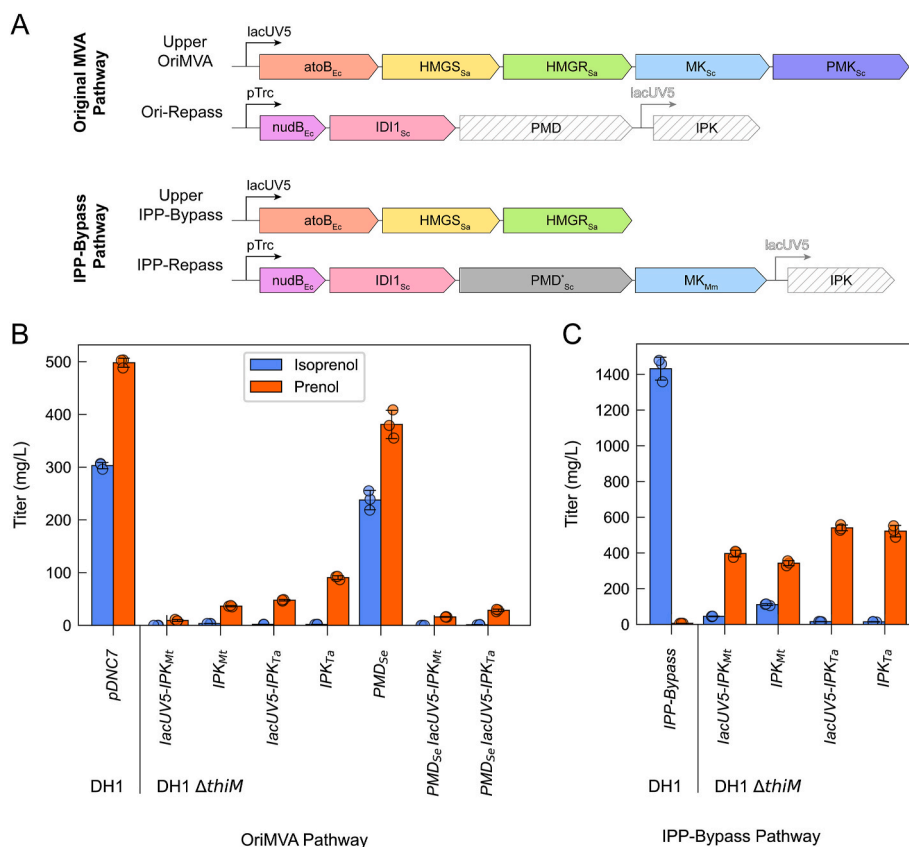


Fig. 2. Production of isoprenol and prenol from different Repass pathway constructs. (A) Plasmid maps of the different MVA pathways as two plasmid systems with pathway variations striped gray. (B) Several decarboxylases (PMD_{Sc} and PMD_{Se}), kinases (IPK_{Ta} and IPK_{Mt}), and operon configurations were explored in the Ori-Repass pathway and compared to a control, pDNC7. (C) IPP-Repass pathway configurations with different kinases and operon configurations were again explored and compared to the IPP-Bypass control.

and screening of homologous pathway enzymes. Selected IPKs were cloned downstream of the lower MVA pathway genes (*nudB*, *IDI1_{Sc}* and *MK_{Sc}*) either constitutively or under a secondary *lacUV5* promoter. An alternative *PMD* from *Staphylococcus epidermidis* (PMD_{Se}) was also evaluated owing to its more stringent selectivity towards MVAPP over MVAP (Kang et al., 2016). Isoprenol, prenol, and combined isopentenols (i.e., the sum of isoprenol and prenol) were compared to control strains which lacked IPK expression (Carruthers et al., 2023) (Fig. 2).

Polycistronic expression of IPK_{Ta} with the OriMVA pathway yielded a 50:1 ratio of prenol to isoprenol achieving a final titer of 90.7 mg/L. Although 4.5-fold lower prenol titer and 7.2-fold lower total isopentenols compared to the pDNC7 control strain, the enrichment of prenol over isoprenol validated that the polycistronic IPK_{Ta} was more selective towards IP than DMAP *in vivo*, thereby driving prenol production. Expressing IPK_{Ta} or IPK_{Mt} under a secondary *lacUV5* promoter significantly reduced isopentenol titers. The observed titer reduction may stem from higher IPK expression, which leads to more stringent diphosphate and monophosphate recycling. Previous studies have also reported poor IPK solubility in *E. coli* (Clomburg et al., 2019) such that attenuating expression may be more favorable. Substitution of PMD_{Sc} with PMD_{Se} yielded lower overall isopentenol production both with and without IPK_{Ta} expression. As a result, the best Ori-Repass circuit involved polycistronic IPK_{Ta} expression in an operon with *NudB_{Ec}*, *IDI1_{Sc}*, and PMD_{Sc} .

Following the success of the Ori-Repass pathway, we then explored whether the IPP-Bypass pathway could be harnessed to generate prenol (Fig. 2C). Prenol production from the IPP-Bypass was intuitively unlikely owing to the single enzymatic step required to convert IP to isoprenol. Nonetheless, we hypothesized that the affinity of IPK towards IP over DMAP could drive prenol generation. Indeed, when paired with the

IPP-Bypass pathway both IPKs again efficiently converted IP to IPP, achieving prenol titers of 342.9 mg/L and 522.2 mg/L at a ratio of 3:1 and 36:1 prenol to isoprenol for IPK_{Mt} and IPK_{Ta} , respectively. As in the OriMVA pathway, the expression of IPK_{Mt} yielded lower, less pure prenol titers compared to IPK_{Ta} . Expression of IPK_{Ta} under a secondary *lacUV5* promoter produced marginally higher prenol compared to its polycistronic counterpart ($p = 0.28$). The polycistronic IPK_{Ta} configuration was selected for future pathway engineering to facilitate inclusion of other genes under the secondary promoter (e.g., *ATF1*, *acPT1*, *GPPS*, etc.). This configuration is also more comparable to the Ori-Repass pathway. Although producing 2.7-fold lower total isopentenols compared to the control, the IPP-Repass strain harboring IPK_{Ta} yielded the highest and purest MVA-derived prenol to date.

The *in vivo* selectivity of IPK_{Mt} and IPK_{Ta} towards DMAP over IP was broadly reflective of published *in vitro* data (Chen and Poulter, 2010). Specifically, the OriMVA pathway yielded 11-fold and 50-fold more prenol while the IPP-Bypass pathway yielded 3-fold and 36-fold more prenol when paired with IPK_{Ta} or IPK_{Mt} , respectively. Characterized by their polycistronic expression of *IDI1_{Sc}*, IPK_{Ta} , and *NudB_{Ec}*, these initial pathway designs established the baseline Ori-Repass and IPP-Repass pathways.

3.2. Modeling the repass pathways

Prenyl/isopentenyl diphosphate recycling is the crux of the repass pathways, however the intracellular diphosphate ratio depends on various factors, including enzyme activity, pathway feedback inhibition, growth phase, precursor toxicity, and MEP/MVA pathway coexpression (George et al., 2018; Martin et al., 2003; Ma et al., 2011). High resolution quantification of monophosphate and diphosphate intermediates is

complicated by the chromatographic challenge of separating isomers. Nonetheless, several studies have quantified IPP/DMAPP ratios, finding that the native MEP pathway generates 5:1 IPP:DMAPP, equilibrating to 3:7 with addition of native IDI (Rohdich et al., 2003). Few studies have quantified IP:DMAP ratios. While the native IPP:DMAPP ratio is supported by in vivo studies (Zhou et al., 2013), how the ratio shifts in the presence of a heterologous, IPK-coupled MVA pathway is uncertain.

Given these challenges, a simple kinetic model was constructed using Python to assess how enzyme kinetics influence bifurcation of pathway intermediates into their respective alcohols. This approach enabled us to understand the relative impact of each enzyme on pathway engineering without the need for direct metabolite measurements. Each enzyme was assumed to strictly follow Michaelis-Menten enzyme kinetics, devoid of a biological context.

A sensitivity analysis was performed with this kinetic model by randomly varying k_{cat}^* and K_m parameters for each of the eight enzymatic reactions (Fig. 3A). Enzyme concentration, assumed constant, and V_{max} were aggregated into the k_{cat}^* parameter for simplicity. Parameters were varied randomly between 1 and 1000-fold with Latin hypercube sampling (LHS) to broadly reflect kinetic parameters typical of secondary metabolism (Bar-Even et al., 2011). From this sampling, a Monte Carlo simulation was performed by iterating the kinetic model 10,000 times with the LHS parameter set. Finally, a Spearman's rank correlation was conducted for both the Repass pathways to assess the relationship between enzymatic parameters (k_{cat}^* , K_m) and the prenol/isoprenol outputs (Fig. 3A).

In the simplified kinetic model, reactions 1 and 6 describe kinase activity, 2 and 7 describe diphosphatase activity, 3 and 4 describe isomerase activity, and finally 2 and 8 describe monophosphatase activity. The IPP and Ori-Repass pathways were modeled with an initial [IP] or [IPP] of 10 arbitrary units, respectively. Running the model to completion resulted in complete bifurcation of metabolites into either prenol or isoprenol (Fig. 3B). As a result, the Spearman's rank correlation coefficients between the final concentrations of isoprenol and prenol were mostly equal and opposite (Fig. 3C). Coefficients deviate from opposite parity due to simulations with exceptionally slow kinetics. Over 10,000 iterations of the IPP-Repass model, approximately 75% of initial IP was converted to isoprenol while in the Ori-Repass model, 58%

of IPP was converted to isoprenol. The relative fractionation of starting substrate into isoprenol aligns with the relative proximity of the intermediate to the output alcohols.

Crucially, the analysis enabled a clearer understanding of the relative impact of kinetics to the production of either alcohol. In particular, the Ori-Repass is most impacted by conversion of IPP to IP by reaction 2 ($\rho_{Isoprenol} = 0.33$, $\rho_{Prenol} = -0.32$) and the conversion of IPP to DMAPP by reaction 4 ($\rho_{Isoprenol} = -0.32$, $\rho_{Prenol} = 0.33$), which are also reflected by parametric variation of their respective K_m values. Conversely, we saw that reactions 2 and 4 are overshadowed by reactions 1 and 5 in the IPP-Repass pathway for which IPP is converted to IP ($\rho_{Isoprenol} = -0.32$, $\rho_{Prenol} = 0.32$) and IP to Isoprenol ($\rho_{Isoprenol} = -0.32$, $\rho_{Prenol} = 0.30$), respectively. Although markedly weaker, the IPP-Repass pathway also displayed a correlation in reaction 2 ($\rho_{Isoprenol} = 0.23$, $\rho_{Prenol} = 0.22$) and reaction 4 ($\rho_{Isoprenol} = -0.24$, $\rho_{Prenol} = 0.24$). In enzymatic terms, harnessing the Ori-Repass for prenol production is most influenced by the selection of phosphatase and isomerase whereas the IPP-Repass is more strongly influenced by the kinase and unknown phosphatase(s) responsible for the dephosphorylation of monophosphate intermediates. Informed by this kinetic model, we next sought to explore different isomerases and phosphatases that might improve prenol production.

3.2.1. Optimization of the repass pathways

A library of 13 *E. coli* Nudix (Nucleoside diphosphate linked to a variable moiety X) hydrolases were selected for expression with IPK_{Pa} due to their general promiscuity and demonstrable activity on DMAPP/IPP (Bessman, 2019; Chou and Keasling, 2013). While *nudB* is typically expressed in tandem with the Original MVA pathway (Zada et al., 2018) for isopentenol production, prediction of diphosphatase efficacy in directing pathway intermediates towards prenol was uncertain. Over-expression of a monophosphatase was not explored owing to the background efficacy of native *E. coli* monophosphatases for the production of isopentenols (Chou and Keasling, 2012; Kang et al., 2017) (Fig. 2) and the relative importance of the monophosphatase compared to other enzymes in yielding isoprenol over prenol in the kinetic model (Fig. 3).

Another library of isomerases was comprehensively reviewed. IDIs are a broad and ubiquitous class of enzymes typified by two unique isomerization mechanisms (Neti et al., 2018). Although both types

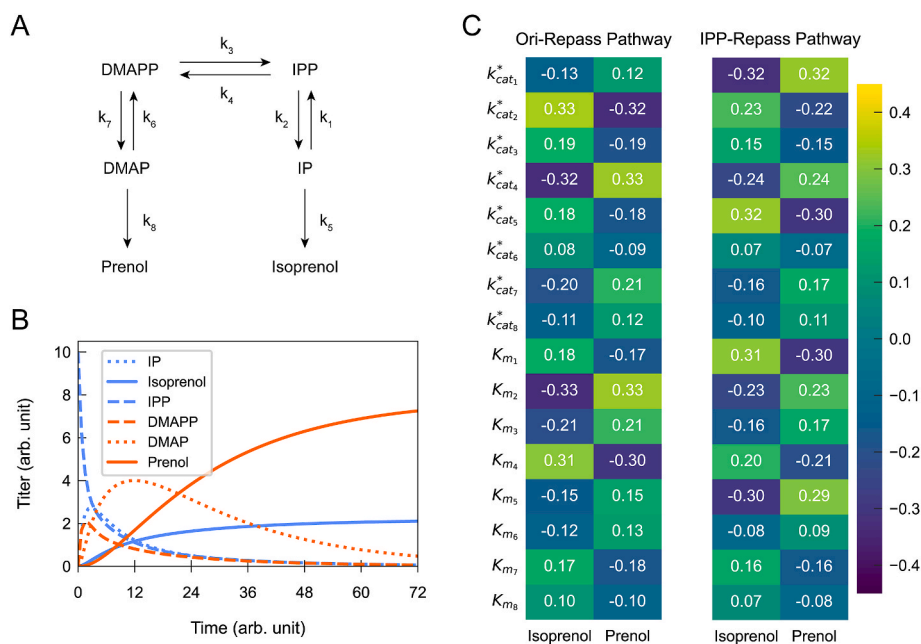


Fig. 3. A kinetic model of the repass pathways. (A) Overall reaction network with each reaction defined by Michaelis-Menten kinetics. (B) Example output from the kinetic model of the Ori-Repass pathway for a given parameter set with an initial IPP concentration of 10 arbitrary units. (C) Spearman's Rank Correlation coefficients for each parameter with regards to the final titer of isoprenol and prenol in the Ori-Repass and IPP-Repass pathways.

proceed via 1,3-proton addition/elimination, they differ in cofactors. Type-1 IDIs (IDI1s) utilize two divalent metal cations to facilitate a putative antarafacial proton elimination/addition (Berthelot et al., 2012). A far more recent discovery, type-2 isomerases (IDI2s) utilize a single divalent cation and are contingent upon a fully reduced flavin mononucleotide (FMN) cofactor. The FMN cofactor then serves as both the acid and the base catalyst for deprotonation-protonation (Neti et al., 2018). Historically, both IDI1 and IDI2 have been harnessed for isoprenoid production with checked improvements in titers. One study demonstrated 1.57-fold improvement of isoprene titer by IDI2 from *Staphylococcus aureus* compared to IDI1_{Sc} with noted reductions in titer by IDI2s from *Bacillus subtilis* and *Bacillus Licheniformis* (Li et al., 2019). Others have demonstrated that IDI2_{Bl} can improve lycopene titer compared to IDI_{Ec}, but IDI2_{Bl} fails to improve astaxanthin yields (Park et al., 2018; Rad et al., 2012). Collectively, these results underline that predicting MVA pathway performance is challenging and non-intuitive.

In light of these disparate mechanisms and difficulty in anticipating selectivity, our isomerase selection included three isomerases from isoprenoid production chassis (*E. coli*; IDI1, *B. subtilis*; IDI2, and *B. licheniformis*; IDI2), two type-2 isomerases from archaea (*M. mazei* and *T. acidophilum*), and two type-2 isomerases from eukaryotes (*S. aureus* and *A. thaliana*). Specifically, the two archaeal IDI2s were selected because their native isomerases and kinases are polycistronic. This arrangement implies a potential preference for DMAPP production, particularly as these organisms lack alternative mechanisms for DMAPP biosynthesis.

The Ori-Repass pathway was initially investigated by examining the Nudix hydrolases along with a control monophosphatase, AphA, all paired with IDI1_{Sc}. Secondly, the 7 isomerases were paired with NudB. All plasmids were cloned into an *E. coli* DH1 Δ *thiM* strain harboring the Upper OriMVA plasmid, JBEL-6829 (Fig. 4).

Two Nudix hydrolases, NudI and NudJ, enhanced prenil titer to 108.7 mg/L and 238.6 mg/L, respectively while maintaining a high prenil:isoprenol ratio (Fig. 4B). In general, most phosphatases led to a substantial decrease in isopentenol titer compared to the NudB control. Notably, NudF, previously reported for its specificity towards DMAPP (Zheng et al., 2013), exhibited significantly lower prenil production in the Ori-Repass pathway compared to the NudB control. The deletion of *thiM* had a negligible overall effect on prenil titer ($p = 0.44$).

Four isomerases, IDI2_{Bs}, IDI2_{Bl}, IDI1_{Ec}, and IDI2_{Sa}, also improved prenil titer. IDI2_{Bl} and IDI2_{Bs} improved prenil titer by 3.3-fold (300.0 mg/L) and 3.1-fold (283.8 mg/L), respectively (Fig. 4C). Despite genetic locality to IDI2 in their archaeal hosts, neither IDI2_{Ta} nor IDI2_{Mm} improved prenil titer. Their reduction in total isopentenol titer is perhaps owing to difficulties in recombinant expression as reported elsewhere (Yoshida et al., 2020). Conversely the other IDI2s increased isopentenol titer, with IDI2_{At} remarkably reversing pathway selectivity. The overproduction of prenil by IDI1_{Ec} is seemingly at odds with the 2-fold decrease in titer reported when paired with the standard OriMVA pathway production scheme (Carruthers et al., 2023). Again, the deviation likely stems from isomerase's role in balancing the diphosphate recursion. Curiously, combining the best combinations of phosphatase and isomerase failed to realize additive titer gains over their isomerases alone (Fig. 4D).

Following exploration of the Ori-Repass pathway, we then explored the same combinations of isomerases and phosphatases in the IPP-Repass pathway configuration, this time coexpressing the Upper IPP-Bypass plasmid, JBEL-17081, in *E. coli* DH1 Δ *thiM* (Fig. 5).

Contrary to the Ori-Repass pathway, the deletion of *thiM* from *E. coli* DH1 yielded a 15% improvement in prenil titer (506.2 mg/L, $p = 0.02$). This difference may arise from the higher overall alcohol titer of the IPP-Repass pathway, where *ThiM* activity becomes more pronounced. Prenil titers in DH1 Δ *thiM* were further improved by substitution of NudB with NudI and NudJ, yielding 541.0 mg/L ($p = 0.04$) and 526.3 mg/L ($p = 0.01$) prenil, respectively (Fig. 5B). NudJ also demonstrated significant selectivity towards prenil:isoprenol with a final ratio of 72:1.

Exploration of different isomerases strictly reduced overall alcohol titer and selectivity (Fig. 5C). The best performing isomerase, IDI2_{Bs}, reduced titer by about 50% compared to IDI1_{Sc}, yielding 294.7 mg/L prenil in a poor 5.1:1 ratio with isoprenol. As in the Ori-Repass pathway, IDI2_{At} dramatically decreased selectivity, IDI2_{Ta} and IDI2_{Mm} both performed poorly and, despite lower overall titer, IDI2_{Sa} maintained strong selectivity towards production.

Of the Nudix hydrolases studied, NudI and NudJ enriched prenil production in both pathways, with NudM (i.e., *yfcD* or *Orf180*) improving titer in the IPP-Repass alone. Despite being from the same family, the best phosphatases maintain an amino acid identity at or below 20%. NudI, NudJ, and NudB have purported activity upon nucleoside di- and triphosphates, though are well known for their promiscuity towards IPP/DMAPP and geranyl diphosphate (GPP). A recent study showed that NudI and NudH maintain higher catalytic activity on DMAPP and GPP compared to its native NDP-x derivatives with NudM also displaying low but significant DMAPP/GPP activity (Bessman, 2019). Phosphatase expression is also contingent on a cellular context such that the overexpression of NudH, which hydrolyses mRNA as one of a number of functions, is detrimental. If, as hypothesized by George et al. (2018), IPP toxicity arises due to hybridization with ATP to form AppI, it is possible that certain hydrolases may relieve toxicity by acting upon AppI. This activity, however, was purportedly not seen by NudM (Bessman, 2019) nor by NudB (George et al., 2018).

As for the isomerases, IDI2_{Bs} and IDI2_{Bl} improved titer in the Ori-Repass pathway alone. Unlike with the Nudix hydrolases, no IDI improved production in the IPP-Repass. Instead, all reduced overall isopentenols and, apart from IDI1_{Sa}, dramatically reduced the selectivity. Even in analogous Ori-MVA C5 alcohol production schemes, IDI1_{Ec} yielded substantially higher isoprenol titer compared to IDI1_{Sc} (Carruthers et al., 2023). Here, the inclusion of IPK reversed those trends. The efficacy or inadequacy of various IDI/nudix permutations in redirecting MVA flux towards prenil seems to hinge upon a nuanced equilibrium of pathway intermediates and enzyme expression, the intricacies of which remain ambiguous.

Following empirical pathway analysis, top performing Repass pathway strains (Ori-Repass with NudB and IDI2_{Bs}; IPP-Repass with NudJ and IDI1_{Sc}) were analyzed for growth and production against representative controls without IPK_{Ta}. Both the IPP-Repass and its control express the Upper IPP-bypass plasmid, however the downstream plasmid of the control is configured pTrc99-nudB-IDI1_{Sc}-MK_{Mm}-PMK_{Sc}. The configuration deviates from the IPP-Repass pathway only in the substitution of PMK_{Sc} with IPK_{Ta} and PMD_{Sc} with PMD_{Sc}^{*}. This configuration does not, therefore, bypass IPP yet remains the best candidate control from which prenil could be generated (Fig. 6).

Both repass pathways exhibited distinct growth defects compared to the controls (Fig. 6A) likely due to the recursion of toxic intermediates. Despite growth inhibition, both pathways demonstrated a strong preference for prenil over isoprenol (Fig. 6B and C). The repass pathways exhibited a lower final OD₆₀₀ compared to the controls, reaching stationary phase at around 36 h, which supports the continued toxicity of IPP/DMAPP and/or the formation of AppI (George et al., 2018). While the Ori-Repass pathway reached a maximum titer by approximately 24 h, the IPP-Repass pathway remarkably continued to produce prenil throughout the stationary phase. As observed previously, the Ori-Repass Control (pDNC7, Upper OriMVA plasmid) displayed marginally higher prenil production compared to isoprenol with the IPP-Repass Control exhibiting a much more gradual, isoprenol-biased alcohol accumulation. Trace amounts of geraniol (25.3 ± 2.6 mg/L) were also detected in IPP-Repass cultures after 72 h, suggesting increased cogeneration and subsequent dephosphorylation of geranyl diphosphate.

Overall, these experiments marked the first instance of highly selective prenil production in a microbial host. While prenil is a valuable compound, we sought to investigate whether prenil or its precursor, DMAPP, could also be utilized in other production pathways, such as the biosynthesis of prenyl acetate and other prenylated compounds.

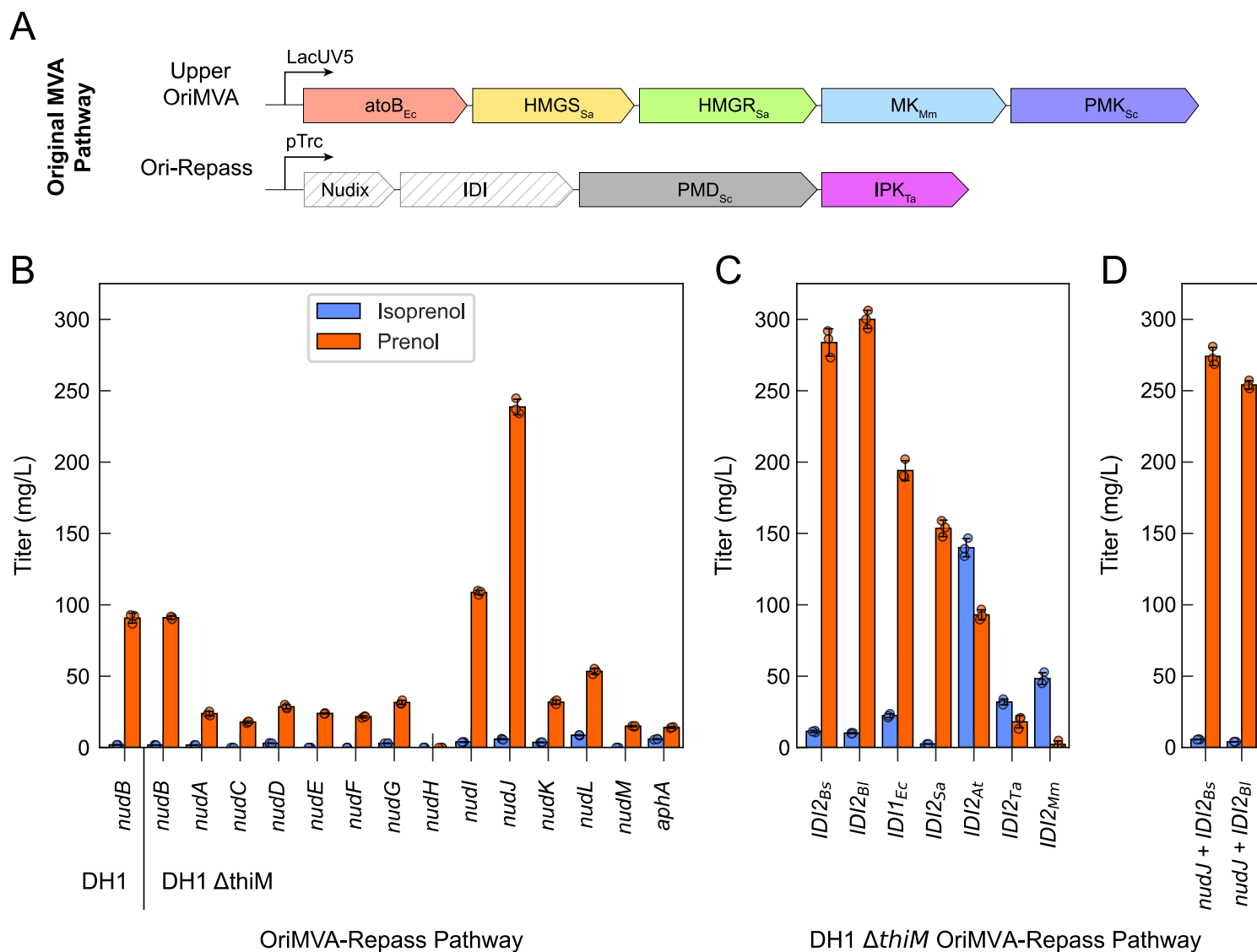


Fig. 4. Prenol and isoprenol production by the Ori-Repass pathway. (A) Plasmid maps depicting the Upper OriMVA and the Ori-Repass plasmids with the variable elements striped gray. (B) Production of isopentenols with different phosphatases and *IDI1_{Sc}*. (C) Production of isopentenols with different isomerases paired with an overexpressed *NudB*. (D) Expression of the best phosphatase, *NudJ*, with the two isomerases, *IDI2_{Bs}* and *IDI2_{Bl}*, associated with the highest prenol titers.

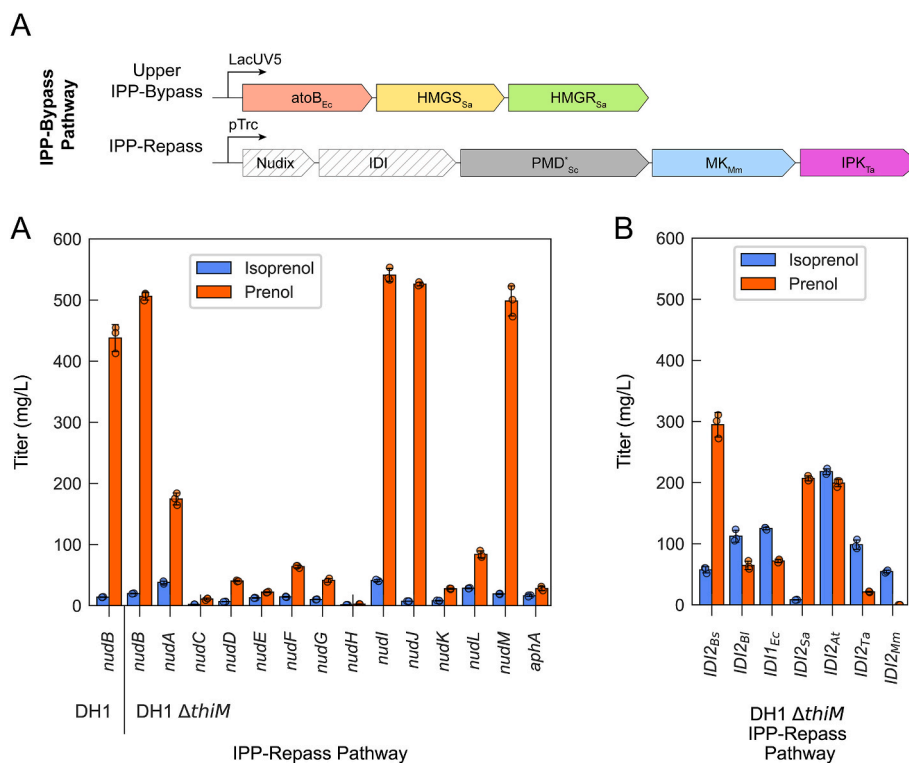


Fig. 5. Prenol and isoprenol production by the IPP-Repass pathway. (A) Plasmid maps depicting the Upper IPP-Bypass and the IPP-Repass plasmids with the variable elements striped gray. (B) Production of isopentenols by pairing different phosphatases with *IDI1_{Sc}*. (C) Production of isopentenols by pairing different isomerases with *NudB* from *E. coli*.

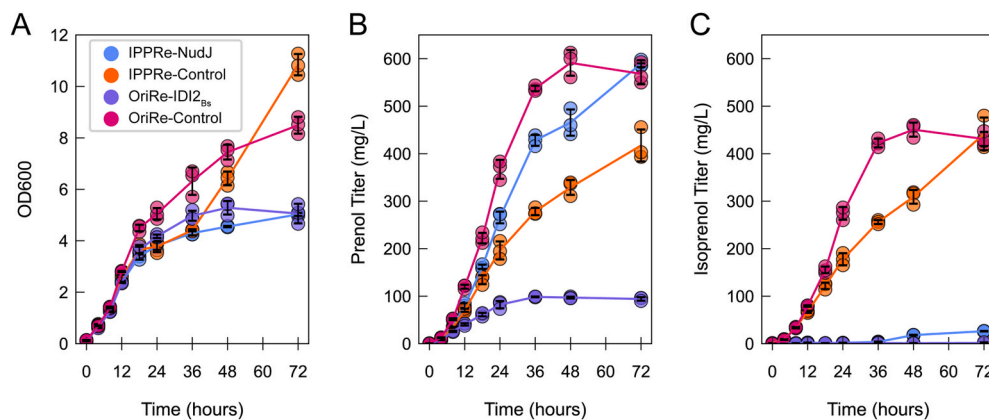


Fig. 6. Growth and alcohol production by the best performing repress pathways and their respective controls lacking *IPK_{Ta}* over 72 h. (A) Growth measured by OD₆₀₀. (B) Prenol production over a 72-h time course. (C) Isoprenol production over a 72-h time course.

3.3. Production of prenyl acetate

Given the success of the repress pathways in generating MVA-derived prenyl, we sought to explore the production of valuable DMAP/DMAPP derivatives. An initial candidate was prenyl acetate, a valuable olefinic blend additive with favorable gasoline blend characteristics (Carruthers et al., 2023). Analogous to the biosynthesis of isoprenyl acetate, ATF1 from *S. cerevisiae* was coexpressed with both the IPP- and Ori-repress pathways (Fig. 7). As the prenyl acetate is more hydrophobic than prenyl, we used organic solvent, oleyl alcohol, as an overlay for in situ product extraction as previously described (Carruthers et al., 2023). The control strain was assembled with a *PMK_{Sc}* in an analogous position to the *IPK_{Ta}* of the Ori-Repress pathway, then coexpressed with the Upper OriMVA plasmid (JBEI-6829). A true IPP-Repress control was not

included owing to the lack of basal prenyl production via the IPP-bypass (Fig. 2) and the similar production between Repass controls (Fig. 6). In all strains, ATF1 was expressed under a secondary lacUV5 promoter and 20% oleyl alcohol overlay was added upon induction to sequester the volatile ester products.

Most of the volatile esters partitioned to the organic phase with the ATF1-Control strain yielding an approximately 1:1 ratio of alcohols and their respective esters. Conversely, both the Ori-Repress and IPP-repress pathways significantly enriched prenyl (214 and 25 mg/L, respectively) and prenyl acetate production (128 and 99 mg/L, respectively) while yielding only trace amounts of isoprenol. While both repress pathways were selective for prenyl acetate, appreciable prenyl accumulation suggests a poor initial balancing of ATF1 with the broader MVA pathway. Expression of ATF1 downstream of *IPK_{Ta}* in the operon

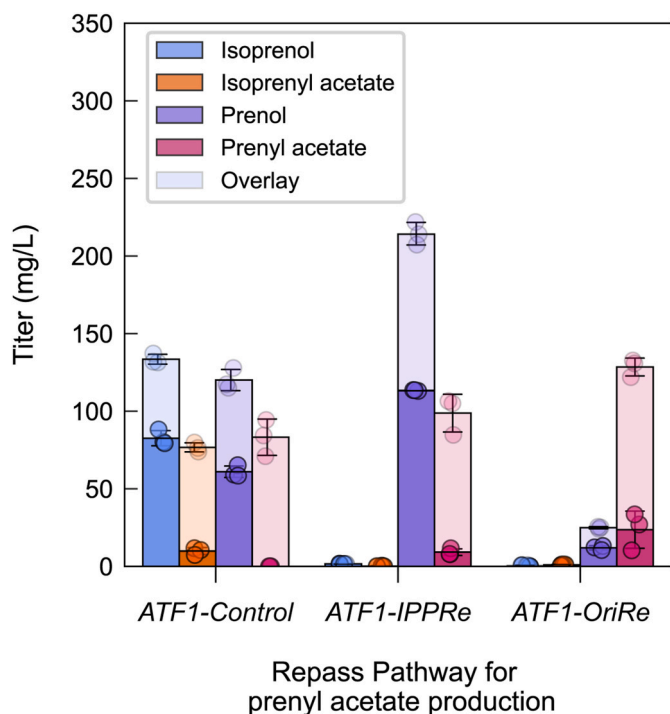


Fig. 7. Production of prenyl acetate by pairing the repress pathways with ATF1 compared to their respective controls. Partitioning of product to the organic leyl alcohol overlay is denoted by shading.

mirroring a high titer isoprenyl acetate strain (Carruthers et al., 2023) failed to improve titer (data not shown). While these strains demonstrate production of repress derived prenyl acetate, higher titers will require further tuning.

3.4. Production of prenylated compounds

Prenylation reactions are characterized as the addition of a hydrophobic prenyl, geranyl, or farnesyl group to a protein or small molecule. Many plants express prenyltransferases that prenylate small often aromatic molecules to generate valuable products as epitomized by bitter acid biosynthesis in *Humulus lupulus* (HIPT1L, HIPT2) as well as in the production of cannabigerolic acid by *Cannabis sativa* (CsPT4) (Luo et al., 2019). A previous report elucidated and expressed a phenylpropane-specific prenyltransferase from *Artemisia capillaris* (acPT1, NCBI: BGG56301.1) in *Saccharomyces cerevisiae* (Munakata et al., 2019). Expression of this enzyme in yeast with p-coumaric acid feeding yielded monoprenylated drupanin and diprenylated artemillin C (Fig. 8A), both of which are potential anticancer precursors (Rodrigues et al., 2021).

Although successful in yeast, acPT1 is a membrane bound eukaryotic protein. Given the challenges of expressing eukaryotic proteins in prokaryotic organisms, we sought to further truncate the previously published, codon-optimized *S. cerevisiae* acPT1co (Δ 150 bp). Informed by DeepLoc-2.0, a tool of characterizing subcellular localization, a further 93 bp was truncated to remove the entirety of the predicted transit peptide to yield acPT1co2 (Δ 243 bp) (Thumuluri et al., 2022). Both genes were then cloned upstream of RFP under an arabinose inducible promoter and expressed in *E. coli* DH1, BL21 and BL21 Star™ to probe protein solubility and localization (Fig. S4). Although RFP fused expression of acPT1co and wild-type acPT1 yielded no discernible fluorescence in any strain, acPT1co2-RFP fluorescence was detected and broadly localized to the cytoplasm of *E. coli* BL21 and partitioned to the soluble fraction upon protein purification.

Next, we designed an IPP-Repass pathway lacking a diphosphatase to

yield DMAPP as the terminal product. We then designed several controls and paired the pathway with acPT1co2 (henceforth termed acPT1) on a tertiary plasmid in BL21 and fed 1 g/L p-coumarate upon induction (Fig. 8C). After 72 h of cultivation, strains were analyzed by HPLC against coumarate and drupanin standards (Fig. 8B).

Only pairing the IPP-Repass with acPT1 yielded detectable levels of prenylated product compared to the controls, with L-arabinose induced acPT1-IPP-Repass generating a final titer of 48.3 mg/L drupanin. Drupanin production was initially validated by LCMS (Fig. S5). Production conditions were then scaled to 1-L. The resulting drupanin product was purified and characterized by NMR (Figs. S6–S9) for conclusive validation. Notably, there was significant growth inhibition in strains expressing the acPT1-IPP-Repass for which the terminal product is DMAPP. This growth inhibition was then exacerbated by acPT1 induction as compared to the RFP control (Fig. 8F). The relative OD₆₀₀ of strains coexpressing acPT1 and either the acPT1-Control or acPT1-IPPre indicates that growth inhibition stemmed largely from acPT1 expression as opposed to drupanin toxicity. A decrease in p-coumaric acid titer as a consequence of drupanin production was not discernible in part due to the coumarate extraction efficiency and the generally low drupanin titer.

Previous studies have reported higher selectivity of acPT1 towards diprenylated artemillin C compared to monoprenylated drupanin in yeast (Rodrigues et al., 2021). In our case, only small peaks were observed at later retention times (r.t. = 29 min and r.t. = 32 min, Fig. S5) where an artemillin C signal might be expected. However, these peaks were too small to warrant purification. It is possible that drupanin was exported before sequential prenulation or that either enzyme truncation or simply the use of *E. coli* as the host chassis may have contributed to selective drupanin production. Indeed, our repress generated drupanin is the highest microbially generated titer to date. Importantly, the demonstrated funneling of DMAPP towards drupanin implies that the recycling of prenyl and isopentenyl mono/di-phosphates could enable precise modulation of precursors for production of monoterpenoids, sesquiterpenoids, or other prenulation reactions.

4. Conclusion

Over-production of DMAPP via the mevalonate pathway has remained a formidable challenge, largely due to the intricate balancing of toxic diphosphate and monophosphate precursors. Nevertheless, DMAPP plays a crucial role not only in the biosynthesis of prenol but also in the initiation of isoprenoid chain elongation and prenulation reactions. To date, the most efficacious strategies for DMAPP bio-production have involved conversion of endogenous prenol or addition of exogenous, petrochemical derived prenol to DMAPP. In this study, we introduced an innovative alternative strategy that employed an isopentenyl monophosphate kinase from *T. acidophilum* to selectively recycle isopentenyl phosphate into isopentenyl diphosphate. We then applied a simple kinetic model to identify bottleneck enzymes and optimize pathways, leading to appreciable improvements in prenol titers for both the Ori-Repass and IPP-Repass pathways. These selective prenol production pathways were further utilized to produce prenol derivatives, successfully yielding the promising fuel additive prenyl acetate and the pharmaceutical compound drupanin. Overall, the demonstrated capacity for the repress pathways to generate isoprenoids and provide prenyl substrates marks a new frontier for MVA pathway engineering.

CRedit authorship contribution statement

David N. Carruthers: Writing – review & editing, Writing – original draft, Visualization, Validation, Methodology, Investigation, Formal analysis, Data curation, Conceptualization. **Isaac Donnell:** Writing – review & editing, Writing – original draft, Methodology, Formal analysis. **Eric Sundstrom:** Writing – review & editing, Project

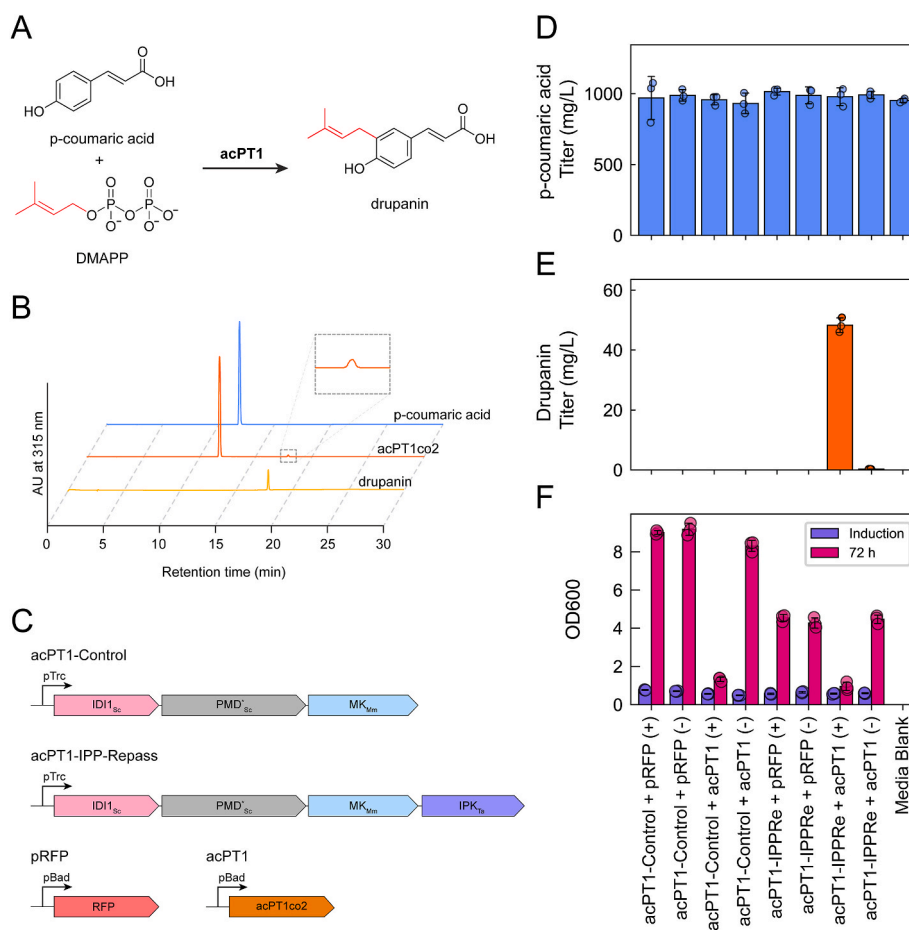


Fig. 8. Production of drupanin via the IPP-Repass pathway. (A) Monoprenylation of p-coumaric acid by acPT1 yields drupanin. (B) HPLC chromatograms of p-coumaric acid standard (r.t. = 11.79 min), an extraction of induced IPP-Repass + acPT1 showing p-coumaric acid and biosynthetic drupanin with magnified view of the drupanin peak, and finally a purified drupanin standard (r.t. = 17.9 min). (C) Plasmid maps of the acPT1-Control and acPT1-IPP-Repass plasmids as well as the tertiary acPT1 and pRFP plasmids used to test drupanin production. All strains also harbored the Upper IPP-Bypass plasmid. (D) p-coumaric acid titer, (E) drupanin titer, and (F) OD₆₀₀ of production cultures at 72 h. Strains labeled acPT1-Control lacked IPK_{Ta} and co-expressed either RFP or acPT1. The ± denotes L-arabinose induction of the tertiary acPT1 or RFP plasmid. The repress pathways were induced in all strains.

administration, Funding acquisition, Conceptualization. **Jay D. Keasling:** Writing – review & editing, Supervision. **Taek Soon Lee:** Writing – review & editing, Writing – original draft, Supervision, Resources, Project administration, Funding acquisition, Data curation, Conceptualization.

Declaration of competing interest

The authors declare that they have no known competing financial interests or personal relationships that could have appeared to influence the work reported in this paper.

Acknowledgements

This work was funded by the Co-Optimization of Fuels & Engines (Co-Optima) project sponsored by the U.S. Department of Energy (DOE) Office of Energy Efficiency and Renewable Energy (EERE), Bioenergy Technologies, and Vehicle Technologies Offices, and the portion of this research was conducted by researchers funded by the DOE Joint Bio-Energy Institute (<http://www.jbei.org>) supported by the U.S. Department of Energy, Office of Science, Office of Biological and Environmental Research, under contract DEAC02-05CH11231 between DOE and Lawrence Berkeley National Laboratory. We thank Drs. Hasan Celik, Raynald Giovine, and Pines Magnetic Resonance Center's Core

NMR Facility (PMRC Core) for spectroscopic assistance. The instruments used in this work were supported by the PMRC Core.

List of abbreviations

AAT	alcohol acetyltransferase
acPT1	<i>Artemisia capillaris</i> prenyltransferase 1
ATF1	alcohol O-acetyltransferase 1
ATP	adenosine triphosphate
CAT	chloramphenicol acetyltransferase
DMAPP	dimethylallyl diphosphate
DMAP	dimethylallyl monophosphate
FMN	flavin mononucleotide;
GC-FID	gas chromatography - flame ionized detection
GC-MS	gas chromatography - mass spectrometry
HMGR	3-Hydroxy-3-methylglutaryl-CoA reductase
HMGS	3-Hydroxy-3-methylglutaryl-CoA-CoA synthase
HPLC	high-performance liquid chromatography
HSQC	heteronuclear single quantum coherence
IDI	isoprenyl diphosphate isomerase
IP	isopentenyl monophosphate
IPK	Isopentenyl monophosphate kinase
IPP	isopentenyl diphosphate
IPPRE	isopentenyl diphosphate repress pathway

MEP	methylerythritol-4-phosphate
MK	mevalonate kinase
MVA	mevalonate
NOESY	nuclear Overhauser effect spectroscopy
NMR	nuclear magnetic resonance
Nudix	nucleoside diphosphate-x;
OriMVA	original mevalonate pathway
OriRe	original repass pathway
PMD	diphosphomevalonate decarboxylase
PMK	mevalonate phosphate kinase
PT	prenyltransferase
RFP	red fluorescent protein

Appendix A. Supplementary data

Supplementary data to this article can be found online at <https://doi.org/10.1016/j.ymben.2025.01.009>.

Data availability

I have shared the link to the code in the SI.

References

- Baba, T., Ara, T., Hasegawa, M., Takai, Y., Okumura, Y., Baba, M., Datsenko, K.A., Tomita, M., Wanner, B.L., Mori, H., 2006. Construction of *Escherichia coli* K-12 in-frame, single-gene knockout mutants: the Keio collection. *Mol. Syst. Biol.* 2, 2006.0008. <https://doi.org/10.1038/msb4100050>.
- Bar-Even, A., Noor, E., Savir, Y., Liebermeister, W., Davidi, D., Tawfik, D.S., Milo, R., 2011. The moderately efficient enzyme: evolutionary and physicochemical trends shaping enzyme parameters. *Biochemistry* 50, 4402–4410. <https://doi.org/10.1021/bi2002289>.
- Baral, N.R., Yang, M., Harvey, B.G., Simmons, B.A., Mukhopadhyay, A., Lee, T.S., Scown, C., 2021. Production cost and carbon footprint of biomass-derived dimethylcyclooctane as a high performance jet fuel blendstock. <https://doi.org/10.26434/chemrxiv.14761002.v1>.
- Berthelot, K., Estevez, Y., Deffieux, A., Peruch, F., 2012. Isopentenyl diphosphate isomerase: a checkpoint to isoprenoid biosynthesis. *Biochimie* 94, 1621–1634. <https://doi.org/10.1016/j.biochi.2012.03.021>.
- Bessman, M.J., 2019. A cryptic activity in the Nudix hydrolase superfamily. *Protein Sci.* 28, 1494–1500. <https://doi.org/10.1002/pro.3666>.
- Carruthers, D.N., Kim, J., Mendez-Perez, D., Monroe, E., Myllybeck, N., Liu, Y., Davis, R.W., Sundstrom, E., Lee, T.S., 2023. Microbial production of high octane and high sensitivity olefinic ester biofuels. *Biotechnol. Biofuels Bioprod* 16, 60. <https://doi.org/10.1186/s13068-02302301-7>.
- Chatzivasileiou, A.O., Ward, V., Edgar, S.M., Stephanopoulos, G., 2019. Two-step pathway for isoprenoid synthesis. *Proc. Natl. Acad. Sci. U.S.A.* 116, 506–511. <https://doi.org/10.1073/pnas.1812935116>.
- Chen, M., Poulter, C.D., 2010. Characterization of thermophilic archaeal isopentenyl phosphate kinases. *Biochemistry* 49, 207–217. <https://doi.org/10.1021/bi9017957>.
- Chen, X., Zhang, C., Zou, R., Stephanopoulos, G., Too, H.-P., 2017. In vitro metabolic engineering of amorpho-4,11-diene biosynthesis at enhanced rate and specific yield of production. *ACS Synth. Biol.* 6, 1691–1700. <https://doi.org/10.1021/acssynbio.6b00377>.
- Cherepanov, P.P., Wackernagel, W., 1995. Gene disruption in *Escherichia coli*: TcR and KmR cassettes with the option of Flp-catalyzed excision of the antibiotic-resistance determinant. *Gene* 158, 9–14. [https://doi.org/10.1016/0378-1119\(95\)00193-A](https://doi.org/10.1016/0378-1119(95)00193-A).
- Chou, H.H., Keasling, J.D., 2013. Programming adaptive control to evolve increased metabolite production. *Nat. Commun.* 4, 2595. <https://doi.org/10.1038/ncomms3595>.
- Chou, H.H., Keasling, J.D., 2012. Synthetic pathway for production of five-carbon alcohols from isopentenyl diphosphate. *Appl. Environ. Microbiol.* 78, 7849–7855. <https://doi.org/10.1128/AEM.01175-12>.
- Clomburg, J.M., Qian, S., Tan, Z., Cheong, S., Gonzalez, R., 2019. The isoprenoid alcohol pathway, a synthetic route for isoprenoid biosynthesis. *Proc. Natl. Acad. Sci. U.S.A.* 116, 12810–12815. <https://doi.org/10.1073/pnas.1821004116>.
- Datta, S., Costantino, N., Court, D.L., 2006. A set of recombinering plasmids for gram-negative bacteria. *Gene* 379, 109–115. <https://doi.org/10.1016/j.gene.2006.04.018>.
- Dellas, N., Thomas, S.T., Manning, G., Noel, J.P., 2013. Discovery of a metabolic alternative to the classical mevalonate pathway. *Elife* 2, e00672. <https://doi.org/10.7554/eLife.00672>.
- George, K.W., Chen, A., Jain, A., Bath, T.S., Baidoo, E.E.K., Wang, G., Adams, P.D., Petzold, C.J., Keasling, J.D., Lee, T.S., 2014. Correlation analysis of targeted proteins and metabolites to assess and engineer microbial isopentenol production. *Biotechnol. Bioeng.* 111, 1648–1658. <https://doi.org/10.1002/bit.25226>.
- George, K.W., Thompson, M.G., Kim, J., Baidoo, E.E.K., Wang, G., Benites, V.T., Petzold, C.J., Chan, L.J.G., Yilmaz, S., Turhanen, P., Adams, P.D., Keasling, J.D., Lee, T.S., 2018. Integrated analysis of isopentenyl pyrophosphate (IPP) toxicity in isoprenoid-producing *Escherichia coli*. *Metab. Eng.* 47, 60–72. <https://doi.org/10.1016/j.ymben.2018.03.004>.
- Kang, A., George, K.W., Wang, G., Baidoo, E., Keasling, J.D., Lee, T.S., 2016. Isopentenyl diphosphate (IPP)-bypass mevalonate pathways for isopentenol production. *Metab. Eng.* 34, 25–35. <https://doi.org/10.1016/j.ymben.2015.12.002>.
- Kang, A., Meadows, C.W., Canu, N., Keasling, J.D., Lee, T.S., 2017. High-throughput enzyme screening platform for the IPP-bypass mevalonate pathway for isopentenol production. *Metab. Eng.* 41, 125–134. <https://doi.org/10.1016/j.ymben.2017.03.010>.
- Kang, A., Mendez-Perez, D., Goh, E.-B., Baidoo, E.E.K., Benites, V.T., Beller, H.R., Keasling, J.D., Adams, P.D., Mukhopadhyay, A., Lee, T.S., 2019. Optimization of the IPP-bypass mevalonate pathway and fed-batch fermentation for the production of isoprenol in *Escherichia coli*. *Metab. Eng.* 56, 85–96. <https://doi.org/10.1016/j.ymben.2019.09.003>.
- Lee, T.S., Krupa, R.A., Zhang, F., Hajimorad, M., Holtz, W.J., Prasad, N., Lee, S.K., Keasling, J.D., 2011. BglBrick vectors and datasheets: a synthetic biology platform for gene expression. *J. Biol. Eng.* 5, 12. <https://doi.org/10.1186/1754-1611-5-12>.
- Liu, Y., Yan, Z., Lu, X., Xiao, D., Jiang, H., 2016. Improving the catalytic activity of isopentenyl phosphate kinase through protein coevolution analysis. *Sci. Rep.* 6, 24117. <https://doi.org/10.1038/srep24117>.
- Li, M., Chen, H., Liu, C., Guo, J., Xu, X., Zhang, H., Nian, R., Xian, M., 2019. Improvement of isoprene production in *Escherichia coli* by rational optimization of RBSs and key enzymes screening. *Microb. Cell Factories* 18, 4. <https://doi.org/10.1186/s12934-018-1051-3>.
- Li, M., Hou, F., Wu, T., Jiang, X., Li, F., Liu, H., Xian, M., Zhang, H., 2020. Recent advances of metabolic engineering strategies in natural isoprenoid production using cell factories. *Nat. Prod. Rep.* 37, 80–99. <https://doi.org/10.1039/c9np00016j>.
- Li, M., Nian, R., Xian, M., Zhang, H., 2018. Metabolic engineering for the production of isoprene and isopentenol by *Escherichia coli*. *Appl. Microbiol. Biotechnol.* 102, 7725–7738. <https://doi.org/10.1007/s00253-018-9200-5>.
- Li, S.-M., 2010. Prenylated indole derivatives from fungi: structure diversity, biological activities, biosynthesis and chemoenzymatic synthesis. *Nat. Prod. Rep.* 27, 57–78. <https://doi.org/10.1039/b909987p>.
- Luo, X., Reiter, M.A., d'Espaux, L., Wong, J., Denby, C.M., Lechner, A., Zhang, Y., Grzybowski, A.T., Harth, S., Lin, W., Lee, H., Yu, C., Shin, J., Deng, K., Benites, V.T., Wang, G., Baidoo, E.E.K., Chen, Y., Dev, I., Petzold, C.J., Keasling, J.D., 2019. Complete biosynthesis of cannabinoids and their unnatural analogues in yeast. *Nature* 567, 123–126. <https://doi.org/10.1038/s41586-019-0978-9>.
- Mabanglo, M.F., Pan, J.-J., Shakyia, B., Poulter, C.D., 2012. Mutagenesis of isopentenyl phosphate kinase to enhance geranyl phosphate kinase activity. *ACS Chem. Biol.* 7, 1241–1246. <https://doi.org/10.1021/cb300106e>.
- Martin, V.J.J., Pitera, D.J., Withers, S.T., Newman, J.D., Keasling, J.D., 2003. Engineering a mevalonate pathway in *Escherichia coli* for production of terpenoids. *Nat. Biotechnol.* 21, 796–802. <https://doi.org/10.1038/nbt833>.
- Ma, S.M., Garcia, D.E., Redding-Johanson, A.M., Friedland, G.D., Chan, R., Bath, T.S., Haliburton, J.R., Chivian, D., Keasling, J.D., Petzold, C.J., Lee, T.S., Chhabra, S.R., 2011. Optimization of a heterologous mevalonate pathway through the use of variant HMG-CoA reductases. *Metab. Eng.* 13, 588–597. <https://doi.org/10.1016/j.ymben.2011.07.001>.
- Monroe, E., Gladden, J., Albrecht, K.O., Bays, J.T., McCormick, R., Davis, R.W., George, A., 2019. Discovery of novel octane hyperboosting phenomenon in prenil biofuel/gasoline blends. *Fuel* 239, 1143–1148. <https://doi.org/10.1016/j.fuel.2018.11.046>.
- Munakata, R., Takemura, T., Tatsumi, K., Moriyoshi, E., Yanagihara, K., Sugiyama, A., Suzuki, H., Seki, H., Muranaka, T., Kawano, N., Yoshimatsu, K., Kawahara, N., Yamaura, T., Grosjean, J., Bourgaud, F., Hehn, A., Yazaki, K., 2019. Isolation of *Artemisia capillaris* membrane-bound di-prenyltransferase for phenylpropanoids and redesign of artemipillin C in yeast. *Commun. Biol.* 2, 384. <https://doi.org/10.1038/s42003-019-0630-0>.
- Neti, S.S., Pan, J.-J., Poulter, C.D., 2018. Mechanistic studies of the protonation-deprotonation reactions for type 1 and type 2 isopentenyl diphosphate:dimethylallyl diphosphate isomerase. *J. Am. Chem. Soc.* 140, 12900–12908. <https://doi.org/10.1021/jacs.8b07274>.
- Park, S.Y., Binkley, R.M., Kim, W.J., Lee, M.H., Lee, S.Y., 2018. Metabolic engineering of *Escherichia coli* for high-level astaxanthin production with high productivity. *Metab. Eng.* 49, 105–115. <https://doi.org/10.1016/j.ymben.2018.08.002>.
- Primak, Y.A., Du, M., Miller, M.C., Wells, D.H., Nielsen, A.T., Weyler, W., Beck, Z.Q., 2011. Characterization of a feedback-resistant mevalonate kinase from the archaeon *Methanosarcina mazei*. *Appl. Environ. Microbiol.* 77, 7772–7778. <https://doi.org/10.1128/AEM.05761-11>.
- Rad, S.A., Zahiri, H.S., Noghabi, K.A., Rajaei, S., Heidari, R., Mojallali, L., 2012. Type 2 IDI performs better than type 1 for improving lycopene production in metabolically engineered *E. coli* strains. *World J. Microbiol. Biotechnol.* 28, 313–321. <https://doi.org/10.1007/s11274-011-0821-4>.
- Rodrigues, D.M., Portapilla, G.B., Silva, G.M., Duarte, A., Rotta, C.G., da Silva, C.H.T., de, P., de Albuquerque, S., Bastos, J.K., Campo, V.L., 2021. Synthesis, antitumor activity and in silico analyses of amino acid derivatives of artemipillin C, drupanin and baccharin from green propolis. *Bioorg. Med. Chem.* 47, 116372. <https://doi.org/10.1016/j.bmc.2021.116372>.
- Rohdich, F., Zepeck, F., Adam, P., Hecht, S., Kaiser, J., Laupitz, R., Gräwert, T., Amslinger, S., Eisenreich, W., Bacher, A., Arigoni, D., 2003. The deoxyxylulose phosphate pathway of isoprenoid biosynthesis: studies on the mechanisms of the reactions catalyzed by IspG and IspH. *Proc. Natl. Acad. Sci. U.S.A.* 100, 1586–1591. <https://doi.org/10.1073/pnas.0337742100>.

- Rosenkoetter, K.E., Kennedy, C.R., Chirik, P.J., Harvey, B.G., 2019. [4 + 4]-cycloaddition of isoprene for the production of high-performance bio-based jet fuel. *Green Chem.* 21, 5616–5623. <https://doi.org/10.1039/C9GC02404B>.
- Thumuluri, V., Almagro Armenteros, J.J., Johansen, A.R., Nielsen, H., Winther, O., 2022. DeepLoc 2.0: multi-label subcellular localization prediction using protein language models. *Nucleic Acids Res.* 50, W228–W234. <https://doi.org/10.1093/nar/gkac278>.
- Tsuruta, H., Paddon, C.J., Eng, D., Lenihan, J.R., Horning, T., Anthony, L.C., Regentin, R., Keasling, J.D., Renninger, N.S., Newman, J.D., 2009. High-level production of amorpho-4,11-diene, a precursor of the antimalarial agent artemisinin, in *Escherichia coli*. *PLoS One* 4, e4489. <https://doi.org/10.1371/journal.pone.0004489>.
- Virtanen, P., Gommers, R., Oliphant, T.E., Haberland, M., Reddy, T., Cournapeau, D., Burovski, E., Peterson, P., Weckesser, W., Bright, J., van der Walt, S.J., Brett, M., Wilson, J., Millman, K.J., Mayorov, N., Nelson, A.R.J., Jones, E., Kern, R., Larson, E., Carey, C.J., SciPy 1.0 Contributors, 2020. SciPy 1.0: fundamental algorithms for scientific computing in Python. *Nat. Methods* 17, 261–272. <https://doi.org/10.1038/s41592-019-0686-2>.
- Wang, F., Lv, X., Xie, W., Zhou, P., Zhu, Y., Yao, Z., Yang, C., Yang, X., Ye, L., Yu, H., 2017. Combining Gal4p-mediated expression enhancement and directed evolution of isoprene synthase to improve isoprene production in *Saccharomyces cerevisiae*. *Metab. Eng.* 39, 257–266. <https://doi.org/10.1016/j.ymben.2016.12.011>.
- Withers, S.T., Gottlieb, S.S., Lieu, B., Newman, J.D., Keasling, J.D., 2007. Identification of isopentenol biosynthetic genes from *Bacillus subtilis* by a screening method based on isoprenoid precursor toxicity. *Appl. Environ. Microbiol.* 73, 6277–6283. <https://doi.org/10.1128/AEM.00861-07>.
- Yoshida, R., Yoshimura, T., Hemmi, H., 2020. Reconstruction of the “archaeal” mevalonate pathway from the methanogenic archaeon *Methanosarcina mazei* in *Escherichia coli* cells. *Appl. Environ. Microbiol.* 86. <https://doi.org/10.1128/AEM.02889-19>.
- Zada, B., Wang, C., Park, J.-B., Jeong, S.-H., Park, J.-E., Singh, H.B., Kim, S.-W., 2018. Metabolic engineering of *Escherichia coli* for production of mixed isoprenoid alcohols and their derivatives. *Biotechnol. Biofuels* 11, 210. <https://doi.org/10.1186/s13068-018-1210-0>.
- Zheng, Y., Liu, Q., Li, L., Qin, W., Yang, J., Zhang, H., Jiang, X., Cheng, T., Liu, W., Xu, X., Xian, M., 2013. Metabolic engineering of *Escherichia coli* for high-specificity production of isoprenol and prenol as next generation of biofuels. *Biotechnol. Biofuels* 6, 57. <https://doi.org/10.1186/1754-6834-6-5>.
- Zhou, C., Li, Z., Wiberley-Bradford, A.E., Weise, S.E., Sharkey, T.D., 2013. Isopentenyl diphosphate and dimethylallyl diphosphate/isopentenyl diphosphate ratio measured with recombinant isopentenyl diphosphate isomerase and isoprene synthase. *Anal. Biochem.* 440, 130–136. <https://doi.org/10.1016/j.ab.2013.05.028>.